Nano Research

Open Access

Research Article

All-carbon-based highly integrated self-powered sensor enabled by flexible perovskite solar cells

Jiashi Wang[1,§], Wenqi Han[1,§], Bing Yin[1] ✉, Wenrui Li[1], Jie Zhang[1], Jiashuo Cheng[1], Lida Liu[1], Yunhan Gao[1], Yudi Wang[1], and Yantao Shi[1,2] ✉

[1] *School of Chemistry, Dalian University of Technology, Dalian 116024, China*
[2] *Frontier Science Center for Smart Materials, Dalian University of Technology, Dalian 116024, China*
[§] *Jiashi Wang and Wenqi Han contributed equally to this work.*

Cite this article: *Nano Research*, **2025**, *18*, 94907801. https://doi.org/10.26599/NR.2025.94907801

ABSTRACT: The rapid expansion of the Internet of Things (IoT) has intensified the need for self-sustaining sensor nodes that circumvent reliance on battery replacements and complex power management. Current off-grid energy solutions often depend on intricate fabrication processes and specialized materials, limiting their scalability and adaptability. Here, we present a self-powered sensing system that leverages the high flexibility and stability of carbon electrodes, combined with the superior photovoltaic performance of perovskite materials, to achieve efficient energy harvesting and storage. Supercapacitors provide durable power buffering, ensuring continuous operation in dynamic environments. Additionally, the device incorporates dual-mode sensing for temperature and mechanical strain, demonstrating reliable and responsive detection capabilities under indoor illumination conditions. By eliminating the need for complex manufacturing processes and corrosion-prone metal components, our design provides a scalable solution for next-generation autonomous sensing networks. This work offers a simplified yet robust approach to developing self-powered IoT nodes, with potential applications in smart infrastructure and environmental monitoring.

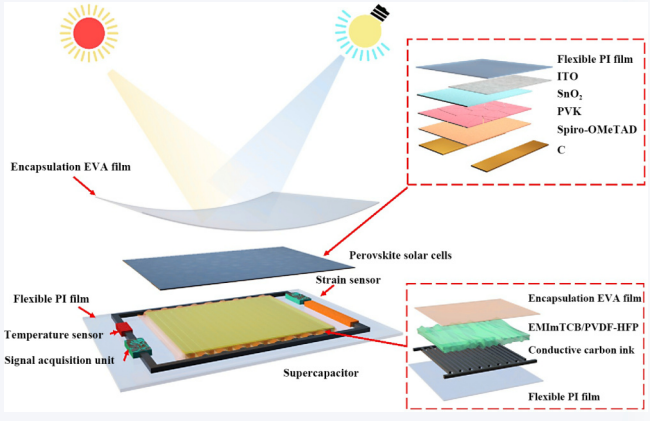

KEYWORDS: carbon-based perovskite solar cells, self-sustaining device, Internet of Things, carbon materials

1 Introduction

Scientific and technological advancements have driven the rapid evolution of the Internet of Things (IoT), establishing it as a crucial link between the physical world and digital networks [1–6]. The IoT's scope of application continues to expand, permeating critical domains, such as smart homes, smart cities, healthcare, agricultural technology, logistics management, and security monitoring [7–10]. The global IoT ecosystem currently relies on 17 billion cable- or battery-dependent nodes, a figure projected to surge by 70% to 29 billion by 2030 [11].

The massive deployment of IoT nodes has introduced challenges related to battery replacement and energy management [12]. To address these issues, researchers have proposed integrating IoT technology with off-grid energy systems, including piezoelectric, triboelectric, thermoelectric generators, fossil fuel engines, and photovoltaic cells, to create self-sustaining devices, such as robots, autonomous vehicles, and satellites [13, 14].

However, current self-sustaining node implementations frequently depend on specialized nanomaterials and elaborate manufacturing protocols. Conventional IoT nodes typically necessitate advanced fabrication methods, including vacuum deposition, photolithography, and thermal compression processing to achieve the necessary integration of functional circuit components [15, 16]. Additionally, the off-grid energy materials used in these systems must meet stringent customization requirements to match the precision circuits. This intricate manufacturing process demands cleanroom facilities and advanced techniques to maintain performance and quality [17]. Another critical consideration is that metals used in such systems—whether as sensors or connection electrodes—often lack corrosion

Received: June 26, 2025; **Revised:** July 12, 2025
Accepted: July 14, 2025

✉Address correspondence to Bing Yin, BingYin@dlut.edu.cn; Yantao Shi, shiyantao@dlut.edu.cn

resistance. This raises concerns about cost, durability, and environmental adaptability, all of which ultimately impact energy storage efficiency [18]. Therefore, developing a universal prototyping and manufacturing method to simplify the production of self-sustaining devices will be critical for their widespread adoption [19–24].

Hybrid organic–inorganic halide perovskite materials are at the forefront of a technological revolution in solar cells [25, 26]. These materials enable the creation of lightweight, ultrathin, and flexible solar cells with record-breaking power densities [27–31]. Perovskite solar cells (PSCs) are particularly notable for their flexible fabrication processes, including compatibility with carbon-based electrodes. This compatibility not only simplifies manufacturing but also opens new avenues for design of flexible power supply [32–34].

By leveraging screen-printing technology, we developed a scalable manufacturing approach to integrate carbon electrode circuits with perovskite-based systems, yielding a streamlined solution for self-sustaining IoT devices. To demonstrate its practicality, we engineered a novel carbon-based self-sustaining photovoltaic monitoring system (CP-S), which seamlessly combines three core functionalities: photovoltaic power generation, energy storage, and environmental monitoring, in a highly integrated design. At its core, the system employs highly efficient carbon-electrode perovskite solar cells for energy harvesting, achieving a 20.64% power conversion efficiency (PCE, test area 7.796 mm^2) under standard test conditions (Air Mass 1.5 (AM 1.5)) while demonstrating excellent operational stability. To ensure continuous operation, we designed a conductive ink-based supercapacitor energy storage module, effectively addressing the energy supply instability caused by intermittent lighting conditions. The system incorporated a multifunctional sensing unit capable of monitoring environmental parameters, exhibiting high sensitivities of 2.51 %·℃$^{-1}$ for temperature and 0.0063 %·με^{-1} (με represents microstrain) for strain under indoor lighting conditions. This integrated system architecture not only overcomes the performance and stability limitations of traditional self-powered systems but also provides a crucial reference for future development of multifunctional, scalable, and self-sustaining electronic devices due to its modular design philosophy.

2 Experimental

2.1 Materials and reagents

Unless mentioned otherwise, all the chemicals were used as received, including $SnCl_2{\cdot}2H_2O$ (98%, Alfa Aesar), $CH(NH_2)_2I$ (FAI, Xi'an Polymer Light Technology Corp), PbI_2 (99.99%, TCI), $PbBr_2$ (> 98.0%, TCI), CH_3NH_3Cl (MACl, Xi'an Polymer Light Technology Corp), 2,2',7,7'-tetrakis(N,N-di-p-methoxyphenyl-amine)-9,9'-spirobifluorene (Spiro-OMeTAD, 99.7%, Lumtec), 4-tert-butylpyridine (TBP, 96%, Sigma Aldrich), lithium bis((trifluoromethyl)sulfonyl)imide (Li-TFSI, 99.95%, Sigma Aldrich), isopropanol (99.5%, Sigma Aldrich), dimethyl sulfoxide (DMSO, 99.9%, Sigma Aldrich), dimethylformamide (DMF, 99.8%, Sigma Aldrich), acetonitrile (99.8%, Sigma Aldrich), chlorobenzene (CB, 99.8%, Sigma Aldrich), deionized water, ethanol (Sinopharm Chemical Reagent Co., Ltd.), acetone (Sinopharm Chemical Reagent Co., Ltd.), carbon nanotubes (CNT, Shenzhen Nanport Co., Ltd.), and graphene (XFNANO Materials Tech Co., Ltd.). ITO (7 Ω·sq^{-1}) was purchased from Suzhou Shangyang Solar Technology Co., Ltd. Conductive ink was purchased from Shenzhen Tengxin New Materials Technology Co., Ltd. Polyvinyl alcohol, poly(vinylidene fluoride-co-hexafluoropropylene) (PVDF-HFP), and 1-ethyl-3-methylimidazole tetrafluoroborate (EMImTCB) were purchased from McLean. Poly(3,4-ethylenedioxythiophene):polystyrenesulfonic acid (PEDOT:PSS) was purchased from Sigma Aldrich.

2.2 Screen-printing of the sensing circuit

The flexible sensing module was fabricated using the screen-printing method to prepare capacitors and bottom circuits. A polyimide (PI) substrate underwent sequential ultrasonic cleaning with cleaning solution, deionized water, ethanol, acetone, and isopropanol (15 min each), followed by drying at 60 ℃ for 20 min and ultraviolet (UV)-ozone treatment for 20 min. After fixing the patterned screen-printing stencil, carbon electrode was doctor-bladed onto the PI substrate and cured at 120 ℃ for 10 min. An electrolyte solution was prepared by dissolving PVDF-HFP in acetone under stirring for 3 h, followed by adding EMImTCB (4:1 mass ratio) and stirring for 12 h. The solution was drop-cast onto the interdigital electrodes, and acetone was evaporated to form a gel electrolyte.

The sensing unit comprised a temperature sensor and a strain sensor. The temperature sensor was fabricated by drop-casting a PEDOT:PSS/CNT hybrid solution (30 mg CNT and 0.5 mL PSS in 10 mL water, ultrasonically mixed and then blended with 1.3 wt.% PEDOT:PSS at a ratio of 1:7) followed by curing at 70 ℃. The strain sensor was prepared by mixing graphite powder with methylcellulose (5:1 mass ratio) in deionized water (1:10 mass ratio), stirring into an electrode-like graphite gel. The graphite gel was coated onto the sensing region and dried at 50 ℃ for 5 min to form a dense sensitive layer. The micro/nanoscale cracks generated during the drying process endowed the layer with strain-responsive characteristics.

2.3 Flexible perovskite device fabrication

Perovskite devices were prepared on PI/indium-tin oxide (ITO) substrate. The PI/ITO substrate was sequentially cleaned ultrasonically using detergent solution, deionized water, anhydrous ethanol, and isopropanol (15 min each), followed by UV-ozone treatment for 15 min. A 3 wt.% SnO_2 colloidal dispersion (diluted in deionized water) was spin-coated onto the PI/ITO substrate at 4000 rpm for 30 s and subsequently annealed at 170 ℃ for 40 min.

The perovskite layer was fabricated using a two-step method within a nitrogen-filled glove box. Initially, a 1.5 M PbI_2 solution in DMF and DMSO (9:1 volume ratio) was coated on the PI/ITO/SnO_2 substrate at 1500 rpm for 30 s, followed by a 70 ℃ annealing for 60 s. After cooling, 100 μL of an organic salt solution (formamidinium iodide (FAI) and MACl dissolved in 3 mL isopropyl alcohol (IPA)) was applied at 1700 rpm for 25 s. The film underwent sequential annealing at 90 ℃ for 25 s and at 150 ℃ for 15 min in ambient air with 30%–40% humidity.

The hole transport layer (HTL) precursor, comprising 72.3 mg Spiro-OMeTAD, 28.8 mL 4-tert-butylpyridine, and 17.5 mL lithium bis((trifluoromethyl)sulfonyl)imide solution in acetonitrile (520 mg·mL^{-1}), was prepared in 1 mL CB and deposited by spin coating at 4000 rpm for 30 s. Subsequently, 200 μL of a graphene dispersion (1 mg·mL^{-1} in IPA) was spray-coated onto the Spiro-OMeTAD layer. Thermal curing at 85 ℃ was then performed to facilitate solvent evaporation, resulting in half-cell A (ITO/SnO_2/formamidinium lead iodide ($FAPbI_3$)/Spiro-OMeTAD/graphene). Finally, conductive carbon paste was blade-

coated onto PI substrate using the screen-printing method, followed by curing at 100 °C to obtain half-cell B.

The conductive carbon paste surface of half-cell B was precisely aligned onto the graphene electrode of half-cell A (with half-cell A positioned beneath half-cell B). Subsequently, an ethylene-vinyl acetate (EVA) film was overlaid onto half-cell B. The stack was then laminated under appropriate pressure using a thermal press. During this process, the EVA layer was thermally activated, creating a hermetic bonding interface between half-cell A and half-cell B to form the complete monolithic photovoltaic device. For integrated CP-S devices, the fabrication process follows identical encapsulation and lamination steps, with half-cell B simply replaced by the capacitive sensing layer specific to the CP-S architecture.

3 Results and discussion

CP-S consists of two functional modules: a carbon-based PSC and a supercapacitor with sensing layer, integrated through a vertically interconnected architecture to achieve functional synergy (Fig. 1(a) and Fig. S1 in the Electronic Supplementary Material (ESM)). The supercapacitor with sensor layer utilizes PI as the flexible substrate, while EVA serves as the encapsulation layer. Through optimized screen-printing, a low-resistance conductive carbon electrode network is precisely fabricated on the PI substrate. Scanning electron microscopy (SEM) image (Fig. 1(b)) reveals that the closely interfaced nano-sized carbon particles in the graphene electrode significantly enhance vertical charge extraction efficiency, thereby optimizing charge transport dynamics (Fig. S2 in the ESM).

The fabrication of the CP-S involves three key steps: First, conductive carbon electrodes are patterned via template-assisted screen printing. Figure 1(c) shows the SEM image of the prepared conductive carbon electrode. Second, the EMImTCB/PVDF-HFP gel electrolyte is injected, followed by localized encapsulation with a transparent EVA layer to stabilize the electrolyte interface and prevent leakage. Finally, the assembly of PSC and supercapacitors is achieved through thermal EVA, against moisture and mechanical stress (Fig. 1(d)).

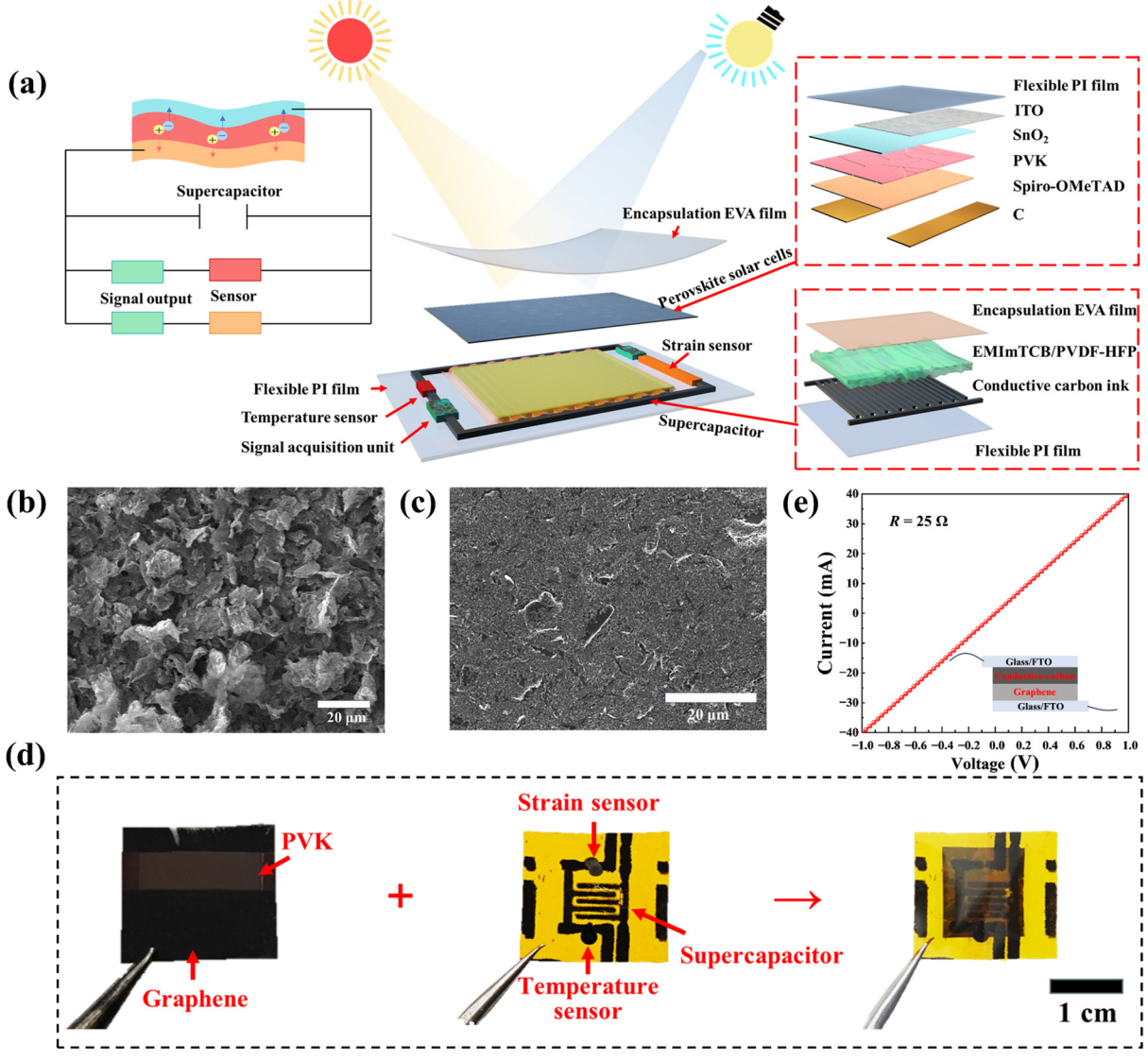

Figure 1 The framework of CP-S. (a) Vertical interconnection architecture schematic diagram: The carbon-based self-powered sensing system consists of two core functional modules: carbon-based PSC and thin-film capacitive sensing layers. (b) SEM image of graphene electrode. (c) SEM image of conductive carbon electrode. (d) Assemble CP-S devices through thermal compression. (e) The *I*–*V* curve of the graphene/carbon electrode hybrid electrode.

The current–voltage (*I*–*V*) characterization (Fig. 1(e)) demonstrates that the graphene/carbon hybrid electrode exhibits both superior vertical charge extraction capability. In addition, through four-probe resistance testing (Fig. S3 in the ESM), the conductive carbon electrode demonstrates highly efficient lateral charge transport capability and can effectively transfer electrons, resulting in significantly reduced interfacial contact resistance, improved charge collection efficiency, and minimized energy loss.

3.1 Graphene-carbon electrodes for stable PSCs

Perovskite materials have demonstrated unique potential in photovoltaic devices due to their precisely tunable light absorption properties and excellent charge transport characteristics. In this study, to investigate the actual working state of carbon-based perovskite solar cells in CP-S, half-cell A was prepared by spraying graphene on the surface of PI/ITO/SnO_2/perovskite/Spiro-OMeTAD, and half-cell B was constructed by scraping conductive carbon paste on PI films. Then, the two independent half-cells were stacked together to form a complete double-carbon module perovskite solar cell (Fig. 2(a)).

Half-cell A can be seen from the cross-sectional SEM image (Fig. 2(b)) that perovskite has a vertically arranged crystal structure and forms a dense contact with the graphene top electrode. In the Raman spectrum of Fig. 2(c), the G-band at 1589 cm^{-1} corresponds to the in-plane vibration of sp^2 hybridized carbon atoms. This suggests that the carbon electrode is composed of graphene. The PSC device based on graphene electrode achieved a PCE of 20.64% (7.796 mm^2). Its open-circuit voltage (V_{OC}) is 1.09 V, the fill factor (FF) is 74.98%, and the short-circuit current density (J_{SC}) is 25.24 $mA·cm^{-2}$ (Fig. 2(d) and Fig. S4 in the ESM). The external quantum efficiency (EQE) curves show an approximate integral of J_{SC} 24.15 $mA·cm^{-2}$ (Fig. 2(e)). Figure 2(f) shows the steady-state output photocurrent and PCE of the CP-S, with a photocurrent of 20.81 $mA·cm^{-2}$ under a bias of 0.94 V and finally yielding steady-state PCE of 19.58%. Considering that CP-S needs to collect information in various environments, the long-term stability of PSC is of crucial importance. We conducted a long-term aging test on it in the N_2 atmosphere. After 1100 h, the PCE of the carbon-based device was 95.03% of the original, while in contrast, the PCE of the metal-based device was only 67.17% of the original. The excellent stability of carbon-based devices makes it possible for the long-term stable operation of CP-S (Fig. 2(g)). Concurrently, for reliable operation in real-world environments, stable PCE of the PSCs is essential to sustain the CP-S system. Our encapsulated PSCs underwent continuous monitoring under controlled conditions

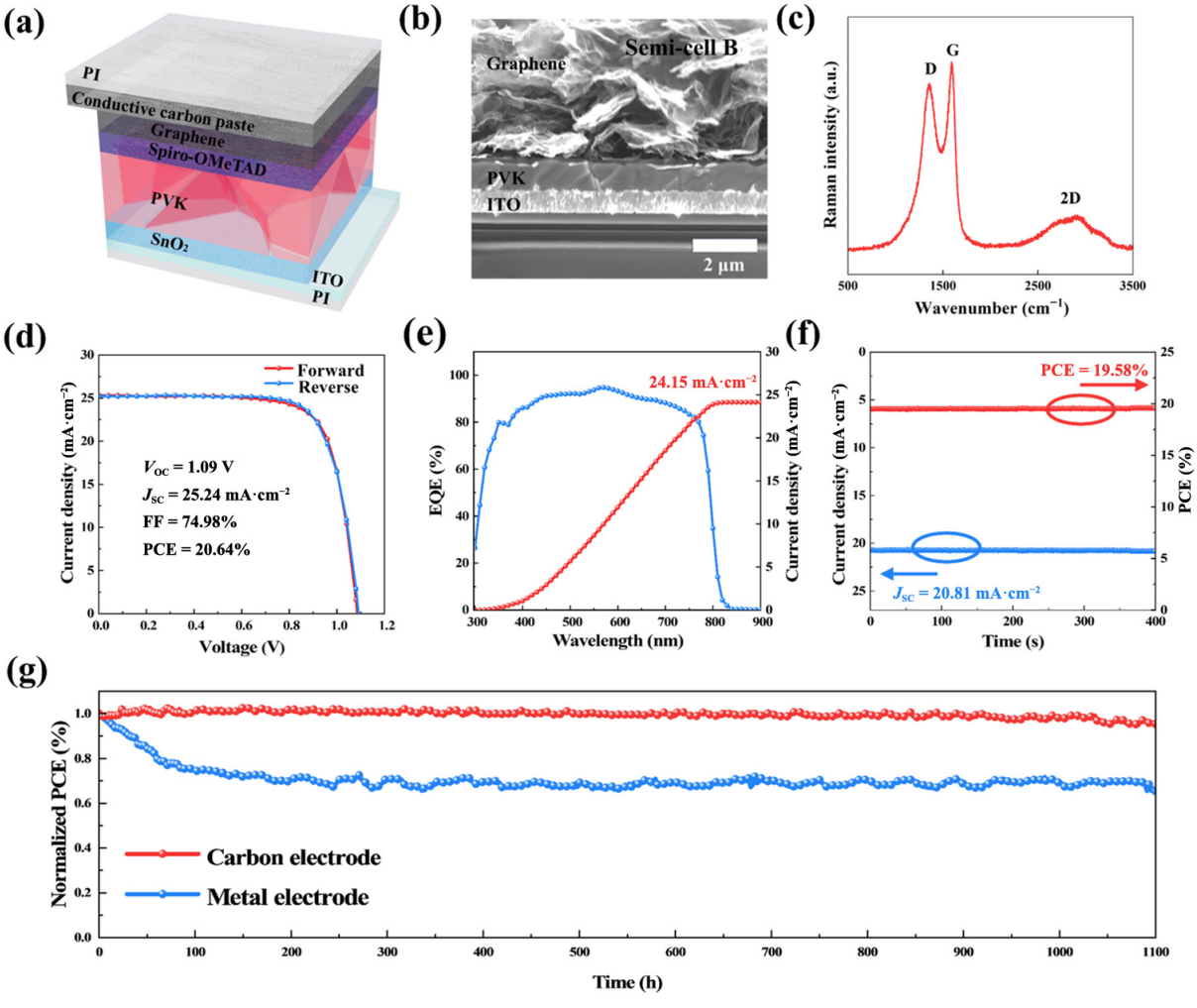

Figure 2 Energy conversion architecture of CP-S. (a) Structural diagram of perovskite solar cells with dual-carbon modules. (b) SEM image of the surface of half-cell A. (c) Raman spectrum of the graphene electrode. (d) PCE curves of PSC. (e) The EQE (blue) and the integrated current density (red) curves of PSC. (f) PSC steady-state output test. (g) PSC long-term stability test: carbon-based (red) and metal-based (blue).

(30% relative humidity, 30 °C), demonstrating remarkable durability by retaining 95.73% of their initial efficiency after 1250 h of aging (Fig. S5 in the ESM).

3.2 Highly robust screen-printed carbon-based supercapacitors

Supercapacitors offer significant promise for wearable electronics due to their high energy storage capacity and mechanical flexibility. This study fabricated high-performance carbon-based electrodes using screen-printing technology (Fig. 3(a) and Fig. S6 in the ESM). Benefiting from carbon's intrinsic conductivity and the continuous conductive network formed during printing, the electrodes exhibited excellent charge transfer properties. Supercapacitors were assembled using EMImTCB/PVDF-HFP electrolyte. Electrochemical characterization revealed efficient charge storage mechanisms. Cyclic voltammetry (CV, Fig. 3(b)) showed quasi-rectangular curves, characteristic of electric double-layer capacitor (EDLC) behavior, across scan rates from 5 to 100 $mV \cdot s^{-1}$. This shape retention at all rates confirms rapid charge propagation kinetics. Consistent with CV results, galvanostatic charge–discharge (GCD, Fig. 3(c)) at 2 $mA \cdot cm^{-2}$ yielded a specific capacitance of 4.8 $mF \cdot cm^{-2}$, indicating uniform electrochemical kinetics. Furthermore, the specific capacitance increased from 4.5 to 2.0 $mF \cdot cm^{-2}$ as the scan rate rose from 5 to 100 $mV \cdot s^{-1}$, highlighting superior rate capability. This stable capacitive performance across varying scan rates confirms EDLC-dominant storage and underpins practical application in dynamic environments.

Mechanical reliability was rigorously assessed. The capacitance retention under different bending degrees is shown in Fig. 3(d), and there is no attenuation of capacity after bending at different bending degrees. We also tested the device for long-term use, and it was bent at a bending angle of 90°. Remarkably, the capacitance of 96.52% was retained after 10,000 bending cycles (Fig. 3(e)). Long-term electrochemical stability was confirmed by 10,000 GCD cycles, showing 96% capacitance retention (Fig. 3(f)). These outstanding mechanical and cycling stability metrics meet the demanding requirements for wearable electronics operating under dynamic conditions.

3.3 Self-powered strain and temperature sensors for environmental monitoring

Self-powered sensors hold significant importance in smart homes, smart cities, and environmental monitoring, where precise detection of ambient changes is critical. In this study, we developed two types of self-powered sensors: a methylcellulose-based strain sensor (Fig. S7 in the ESM) and a PEDOT:PSS-based temperature sensor (Fig. S8 in the ESM). These sensors operate on the principle of resistance variation, dynamically adjusting their resistance in response to external stimuli.

The temperature sensor was characterized across the biologically relevant range of 25–45 °C (Fig. 4(a)), demonstrating stable operation with a sensitivity of 2.51 $\%\cdot°C^{-1}$ (Fig. 4(b)). Concurrently, the strain sensor exhibited robust performance up to 1890 με (Fig. 4(c)), displaying a monotonic increase in current and decrease in resistance with applied strain (sensitivity: 0.0063 $\%\cdot\mu\varepsilon^{-1}$; Fig. 4(d)). For practical deployment, sensor stability under mechanical deformation is paramount. As demonstrated by the step-response curves in Fig. S9(a) in the ESM (methylcellulose strain sensor) and Fig. S9(b) in the ESM (PEDOT:PSS temperature sensor), both components maintained reliable signal output capabilities after 10,000 bending cycles at a 5 mm radius, indicating exceptional fatigue resistance. Further validation comes from the post-cycling sensitivity calibration data (Figs. S9(c) and S9(d) in the ESM), revealing signal deviations of 4.5% for strain detection and

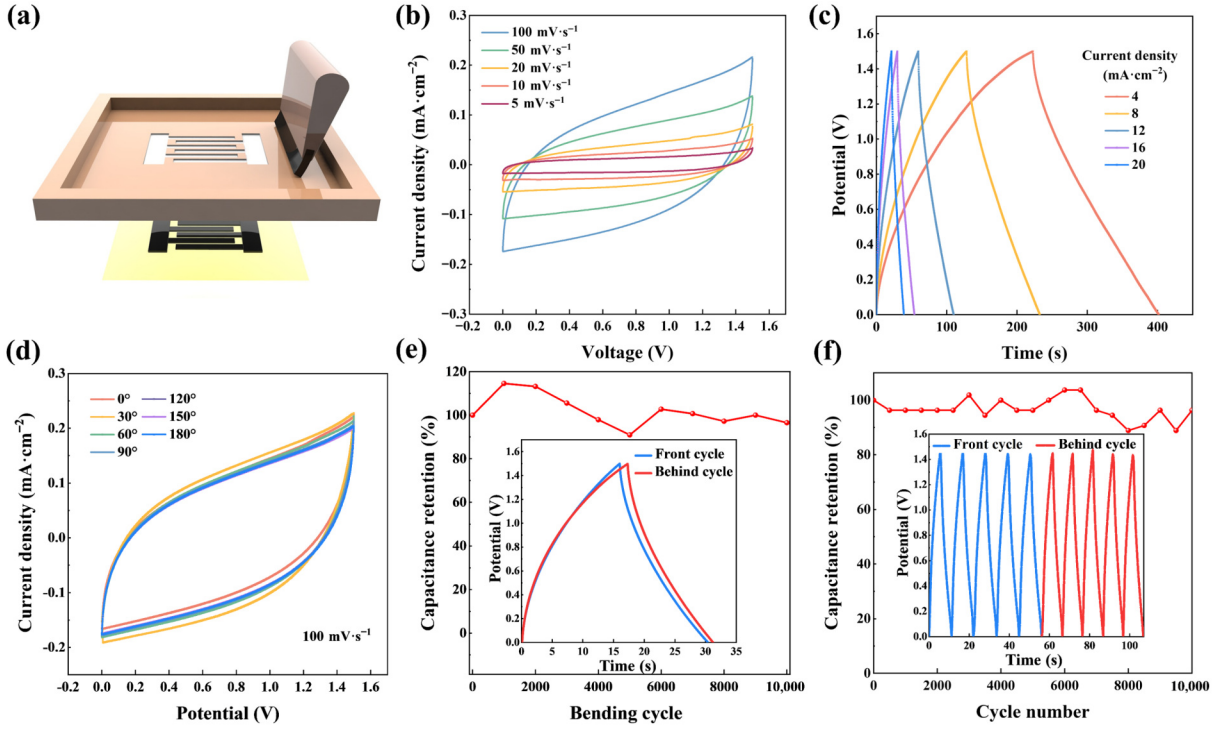

Figure 3 Energy storage device for CP-S. (a) Energy storage unit architecture of self-supplied photovoltaic detection system. (b) Cyclic voltammetry test curves of supercapacitor. (c) Constant current charge and discharge test curves of supercapacitor. (d) Multi-angle dynamic bending test model of supercapacitor. (e) Capacitance retention rate under the number of bending cycles. (f) Constant current charge and discharge test of supercapacitors under long-term working conditions.

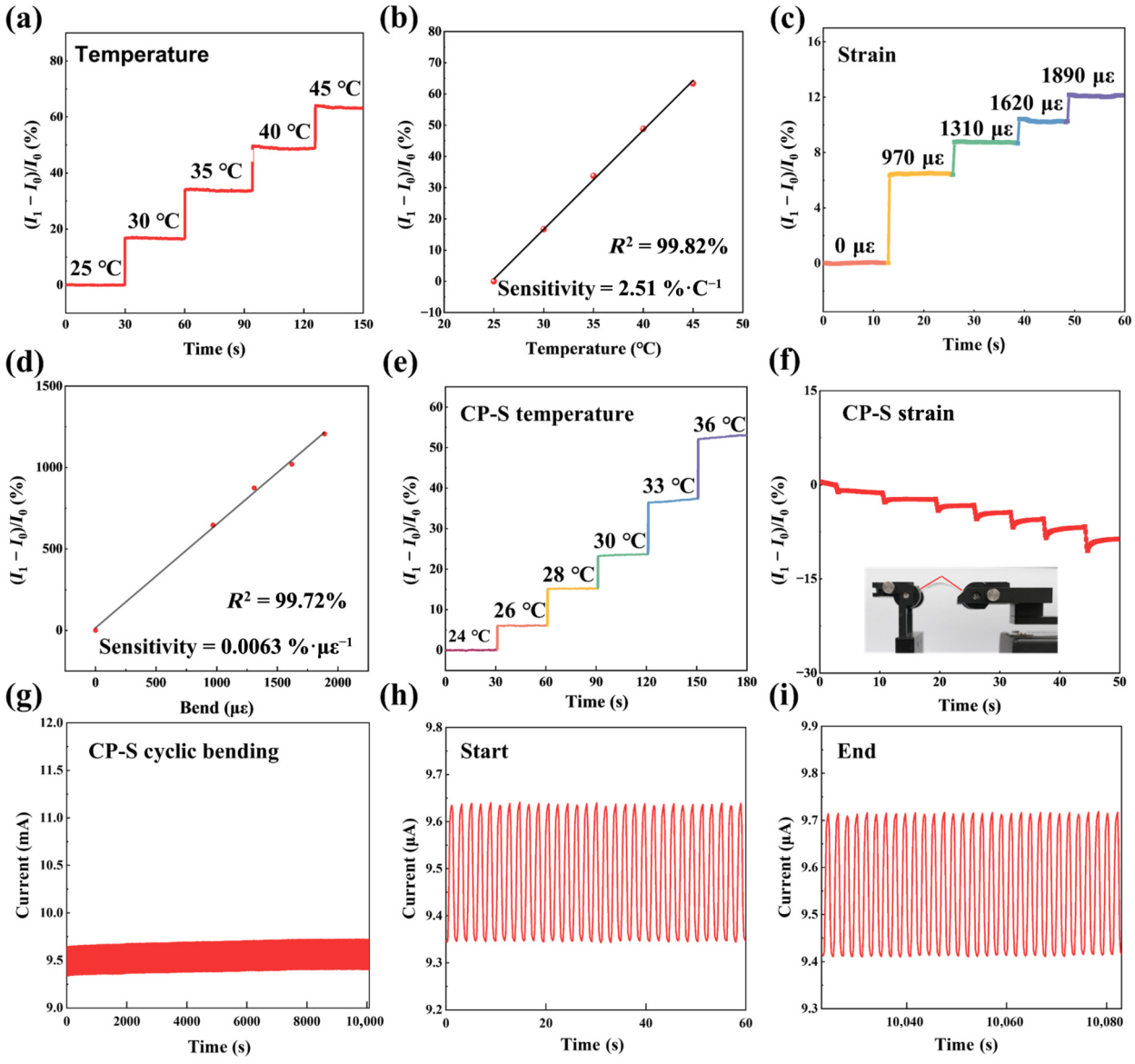

Figure 4 CP-S self-power supply detection. (a) Temperature response step curve of PEDOT:PSS temperature sensor. (b) The sensitivity fitting curve of PEDOT:PSS temperature sensor. (c) Strain response step curve of methyl cellulose strain sensor. (d) The sensitivity fitting curve of methylcellulose strain sensor. (e) The temperature response step curve of CP-S. (f) The strain corresponding to the step curve of CP-S. ((g)–(i)) The cyclic bending curves of CP-S: (h) start and (i) end.

5.2% for temperature sensing. Collectively, these results confirm retention of fundamental sensing capabilities and linear response characteristics even following extreme mechanical stress, validating robust performance in real-world operating environments.

Subsequently, we evaluated the self-powered energy supply of CP-S under indoor lighting conditions (1000 lux). The CP-S module demonstrated an impressive PCE of 35.37% (Fig. S10(a) in the ESM), while the integrated capacitor module achieved rapid charging to 1.1 V in just 12 s (Fig. S10(b) in the ESM). Under indoor illumination, CP-S maintains stable temperature sensing (24–36 °C, Fig. 4(e)) and demonstrates sensitive strain detection (0–2000 με, Fig. 4(f)).

The fabricated CP-S device demonstrated exceptional mechanical durability, exhibiting no detectable signal degradation after 5000 bending cycles at 10 mm radius, confirming its robustness for flexible electronics applications (Figs. 4(g)–4(i)). Through multidimensional optimization and characterization, this work lays a foundation for developing highly stable, practical self-powered environmental monitoring systems.

4 Conclusions

In summary, this work presents a fully integrated, self-powered sensing system combining carbon-based perovskite photovoltaics, supercapacitors with sensing layer to achieve continuous energy harvesting, storage, and signal detection. The hybrid organic–inorganic perovskite solar cells demonstrate power conversion efficiency (20.64%, 7.796 mm^2) and environmental stability (95.03% PCE retention after 1100 h), essential for deformable electronics. Meanwhile, the screen-printed carbon supercapacitors exhibit exceptional energy storage (2.4 F·g^{-1} capacitance) and cycling stability (96.52% retention after 10,000 cycles), enabled by an innovative EMImTCB/PVDF-HFP ionic gel electrolyte.

Unlike conventional metal-based or vacuum-deposited

electrodes, this fully printable carbon electrode system offers superior corrosion resistance, mechanical robustness, and seamless process compatibility, demonstrating that carbon electrodes are not merely a low-cost alternative but a performance-competitive solution for self-powered flexible electronics that paves the way for scalable IoT and wearable applications.

Electronic Supplementary Material: Supplementary material (experimental methods and Figs. S1–S10) is available in the online version of this article at https://doi.org/10.26599/NR.2025.94907801.

Data availability

All data needed to support the conclusions in the paper are presented in the manuscript and the Electronic Supplementary Material. Additional data related to this paper may be requested from the corresponding author upon request.

Acknowledgements

The work was supported by the National Natural Science Foundation of China (Nos. 52272193 and 22304020) and the Fundamental Research Funds for the Central Universities (No. DUT22LAB602).

Declaration of competing interest

All the contributing authors report no conflict of interests in this work.

Author contribution statement

J. S. W.: Data curation, validation, investigation, methodology, writing – original draft. W. Q. H.: Data curation, formal analysis, validation, methodology, writing – original draft. B. Y.: Funding acquisition, project administration, supervision, writing – review & editing. W. R. L.: Investigation, resources, validation. J. Z.: Visualization, methodology, data curation. J. S. C.: Resources, validation. L. D. L.: Formal analysis, visualization. Y. H. G.: Data curation, validation. Y. D. W.: Resources, investigation. Y. T. S.: Conceptualization, funding acquisition, project administration, supervision, writing – review & editing. All the authors have approved the final manuscript.

Use of AI statement

None.

References

[1] Portilla, L.; Loganathan, K.; Faber, H.; Eid, A.; Hester, J. G. D.; Tentzeris, M. M.; Fattori, M.; Cantatore, E.; Jiang, C.; Nathan, A. et al. Wirelessly powered large-area electronics for the Internet of Things. *Nat. Electron.* **2022**, *6*, 10–17.

[2] Polyzoidis, C.; Rogdakis, K.; Kymakis, E. Indoor perovskite photovoltaics for the Internet of Things-challenges and opportunities toward market uptake. *Adv. Energy Mater.* **2021**, *11*, 2101854.

[3] Pecunia, V.; Occhipinti, L. G.; Hoye, R. L. Z. Emerging indoor photovoltaic technologies for sustainable Internet of Things. *Adv. Energy Mater.* **2021**, *11*, 2100698.

[4] Mocrii, D.; Chen, Y. X.; Musilek, P. IoT-based smart homes: A review of system architecture, software, communications, privacy and security. *Internet Things* **2018**, *1–2*, 81–98.

[5] Mathews, I.; Kantareddy, S. N.; Buonassisi, T.; Peters, I. M. Technology and market perspective for indoor photovoltaic cells. *Joule* **2019**, *3*, 1415–1426.

[6] Lei, H.; Xiao, J.; Chen, Y. F.; Jiang, J. W.; Xu, R. J.; Wen, Z.; Dong, B.; Sun, X. H. Bamboo-inspired self-powered triboelectric sensor for touch sensing and sitting posture monitoring. *Nano Energy* **2022**, *91*, 106670.

[7] Celik, Z. B.; Fernandes, E.; Pauley, E.; Tan, G.; McDaniel, P. Program analysis of commodity IoT applications for security and privacy: Challenges and opportunities. *ACM Comput. Surv.* **2020**, *52*, 74.

[8] Qadri, Y. A.; Nauman, A.; Zikria, Y. B.; Vasilakos, A. V.; Kim, S. W. The future of healthcare Internet of Things: A survey of emerging technologies. *IEEE Commun. Surv. Tutorials* **2020**, *22*, 1121–1167.

[9] Yamout, Y.; Yeasar, T. S.; Iqbal, S.; Zulkernine, M. Beyond smart homes: An in-depth analysis of smart aging care system security. *ACM Comput. Surv.* **2024**, *56*, 45.

[10] Nguyen, D. C.; Pathirana, P. N.; Ding, M.; Seneviratne, A. Integration of blockchain and cloud of things: Architecture, applications and challenges. *IEEE Commun. Surv. Tutorials* **2020**, *22*, 2521–2549.

[11] Liu, Z. Q.; Chen, X. Y.; Wang, Z. L. Biopolymer and biomimetic techniques for triboelectric nanogenerators (TENGs). *Adv. Mater.* **2025**, *37*, 2409440.

[12] Chakraborty, A.; Lucarelli, G.; Xu, J.; Skafi, Z.; Castro-Hermosa, S.; Kaveramma, A. B.; Balakrishna, R. G.; Brown, T. M. Photovoltaics for indoor energy harvesting. *Nano Energy* **2024**, *128*, 109932.

[13] Zhang, Y. P.; Wang, L. L.; Zhao, L. J.; Wang, K.; Zheng, Y. Q.; Yuan, Z. Y.; Wang, D. Y.; Fu, X. Y.; Shen, G. Z.; Han, W. Flexible self-powered integrated sensing system with 3D periodic ordered black phosphorus@MXene thin-films. *Adv. Mater.* **2021**, *33*, 2007890.

[14] Pu, X.; Wang, Z. L. Self-charging power system for distributed energy: Beyond the energy storage unit. *Chem. Sci.* **2021**, *12*, 34–49.

[15] Qamar, M. Z.; Khalid, Z.; Shahid, R.; Tsoi, W. C.; Mishra, Y. K.; Kyaw, A. K. K.; Saeed, M. A. Advancement in indoor energy harvesting through flexible perovskite photovoltaics for self-powered IoT applications. *Nano Energy* **2024**, *129*, 109994.

[16] Jahandar, M.; Kim, S.; Lim, D. C. Indoor organic photovoltaics for self-sustaining IoT devices: Progress, challenges, and practicalization. *ChemSusChem* **2021**, *14*, 3449–3474.

[17] Song, Y.; Tay, R. Y.; Li, J. H.; Xu, C. H.; Min, J. H.; Shirzaei Sani, E.; Kim, G.; Heng, W. Z.; Kim, I.; Gao, W. 3D-printed epifluidic electronic skin for machinelearning-powered multimodal health surveillance. *Sci. Adv.* **2023**, *9*, eadi6492.

[18] Saifi, S.; Xiao, X.; Cheng, S. M.; Guo, H. T.; Zhang, J. S.; Müller-Buschbaum, P.; Zhou, G. M.; Xu, X. M.; Cheng, H. M. An ultraflexible energy harvesting-storage system for wearable applications. *Nat. Commun.* **2024**, *15*, 6546.

[19] Yu, L. H.; Yi, Y. Y.; Yao, T.; Song, Y. Z.; Chen, Y. R.; Li, Q. C.; Xia, Z.; Wei, N.; Tian, Z. N.; Nie, B. Q. et al. All VN-graphene architecture derived self-powered wearable sensors for ultrasensitive health monitoring. *Nano Res.* **2019**, *12*, 331–338.

[20] Li, C.; Cong, S.; Tian, Z. N.; Song, Y. Z.; Yu, L. H.; Lu, C.; Shao, Y. L.; Li, J.; Zou, G. F.; Rümmeli, M. H. et al. Flexible perovskite solar cell-driven photo-rechargeable lithium-ion capacitor for self-powered wearable strain sensors. *Nano Energy* **2019**, *60*, 247–256.

[21] Tian, Z. N.; Sun, Z. T.; Shao, Y. Y.; Gao, L.; Huang, R.; Shao, Y. L.; Kaner, R. B.; Sun, J. Y. Ultrafast rechargeable Zn micro-batteries endowing a wearable solar charging system with high overall efficiency. *Energy Environ. Sci.* **2021**, *14*, 1602–1611.

[22] Wang, J. F.; Huang, J. J.; Abdel-Shakour, M.; Liu, T. H.; Wang, X.; Pan, Y. L.; Wang, L. X.; Cui, E. H.; Hu, J. S.; Yang, S. H. et al. Colloidal zeta potential modulation as a handle to control the crystallization kinetics of tin halide perovskites for photovoltaic applications. *Angew. Chem., Int. Ed.* **2024**, *63*, e202317794.

[23] Ma, Q. Y.; Wang, Y. S.; Liu, L. M.; Yang, P.; He, W. J.; Zhang, X.;

Zheng, J. Z.; Ma, M. E.; Wan, M. X.; Yang, Y. Z. et al. One-step dual-additive passivated wide-bandgap perovskites to realize 44.72%-efficient indoor photovoltaics. *Energy Environ. Sci.* **2024**, *17*, 1637–1644.

[24] Li, Y.; Nie, T.; Ren, X. D.; Wu, Y.; Zhang, J.; Zhao, P. J.; Yao, Y. Y.; Liu, Y. C.; Feng, J. S.; Zhao, K. et al. *In situ* formation of 2D perovskite seeding for record-efficiency indoor perovskite photovoltaic devices. *Adv. Mater.* **2024**, *36*, 2306870.

[25] Zhang, W. X.; Guo, X. M.; Cui, Z. B.; Yuan, H. B.; Li, Y. F.; Li, W.; Li, X. D.; Fang, J. F. Strategies for improving efficiency and stability of inverted perovskite solar cells. *Adv. Mater.* **2024**, *36*, 2311025.

[26] Li, F. M.; Wu, D.; Shang, L.; Xia, R.; Zhang, H. R.; Huang, Z. X.; Gong, J.; Mao, L.; Zhang, H.; Sun, Y. Q. et al. Highly efficient monolithic perovskite/perovskite/silicon triple-junction solar cells. *Adv. Mater.* **2024**, *36*, 2311595.

[27] Ali, I.; Islam, M. R.; Yin, J. Y.; Eichhorn, S. J.; Chen, J.; Karim, N.; Afroj, S. Advances in smart photovoltaic textiles. *ACS Nano* **2024**, *18*, 3871–3915.

[28] You, I.; Pau, G.; Salerno, V. M.; Sharma, V. Special issue "Internet of Things for smart homes". *Sensors* **2019**, *19*, 4173.

[29] Yang, L.; Wang, S. B.; Ma, N. G.; Shi, W.; Fang, Z.; Jin, Y. B.; Hou, E. L.; Xu, P.; Cao, F. X.; Li, W. H. et al. Modulating binding strength and acidity of benzene-derivative ligands enables efficient and hysteresis-free perovskite/silicon tandem solar cells. *Angew. Chem., Int. Ed.* **2025**, *64*, e202500350.

[30] Huang, J. H.; Wang, Z.; Hou, M. Y.; Dong, X. L.; Liu, Y.; Wang, Y. G.; Xia, Y. Y. Polyaniline-intercalated manganese dioxide nanolayers as a high-performance cathode material for an aqueous zinc-ion battery. *Nat. Commun.* **2018**, *9*, 2906.

[31] Rind, Y. M.; Raza, M. H.; Zubair, M.; Mehmood, M. Q.; Massoud, Y. Smart energy meters for smart grids, an Internet of Things perspective. *Energies* **2023**, *16*, 1974.

[32] Hu, R. Y.; Chu, L.; Zhang, J.; Li, X. A.; Huang, W. Carbon materials for enhancing charge transport in the advancements of perovskite solar cells. *J. Power Sources* **2017**, *361*, 259–275.

[33] Ferguson, V.; Silva, S. R. P.; Zhang, W. Carbon materials in perovskite solar cells: Prospects and future challenges. *Energy Environ. Mater.* **2019**, *2*, 107–118.

[34] Fagiolari, L.; Bella, F. Carbon-based materials for stable, cheaper and large-scale processable perovskite solar cells. *Energy Environ. Sci.* **2019**, *12*, 3437–3472.